small NANO MICRO

Quantum dots

DOI: 10.1002/smll.200500227

Type-II CdSe/CdTe/ZnTe (Core–Shell–Shell) Quantum Dots with Cascade Band Edges: The Separation of Electron (at CdSe) and Hole (at ZnTe) by the CdTe Layer

Chun-Yen Chen, Chiu-Ting Cheng, Chih-Wei Lai, Ya-Hui Hu, Pi-Tai Chou, Yi-Hsuan Chou, and Hsin-Tien Chiu**

The rational design and synthesis of CdSe/CdTe/ZnTe (core–shell–shell) type-II quantum dots are reported. Their photophysical properties are investigated via the interband CdSe→ZnTe emission and its associated relaxation dynamics. In comparison to the strong CdSe (core only) emission ($\lambda_{max} \approx 550$ nm, $\Phi_f \approx 0.28$), a moderate CdSe→CdTe emission ($\lambda_{max} \approx 1026$ nm, $\Phi_f \approx 1.2 \times 10^{-3}$) and rather weak CdSe→ZnTe interband emission ($\lambda_{max} \approx 1415$ nm, $\Phi_f \approx 1.1 \times 10^{-5}$) are resolved for the CdSe/CdTe/ZnTe structure (3.4/1.8/1.3 nm). Capping CdSe/CdTe with ZnTe results in a distant electron–hole separation between CdSe (electron) and ZnTe (hole) via an intermediate CdTe layer. In the case of the CdSe/CdTe/ZnTe structure, a lifetime as long as 150 ns is observed for the CdSe→ZnTe (1415 nm) emission. This result further indicates an enormously long radiative lifetime of ≈10 ms. Upon excitation of the CdSe/CdTe/ZnTe structure, the long-lived charge separation may further serve as an excellent hole carrier for catalyzing the redox oxidation reaction.

Keywords:
- colloids
- core–shell materials
- quantum dots
- semiconductors
- time-resolved spectroscopy

1. Introduction

As opposed to type-I quantum dots (QDs), in which the energy level of the valence band (conduction band) in the shell is lower (higher) than that of the core, type-II QDs have both valence and conduction bands in the core lower (or higher) than those in the shell materials. Upon electronic excitation, one carrier is predominantly confined to the core, while the other is located at the shell. This spatial separation of charge carriers has led to several characteristic differences from the type-I QDs. Particularly, interband emission is allowable with an energy gap that would otherwise be inaccessible with type-I structures, thus extending the color-tuning capability to the near infrared. Despite well-documented studies regarding type-I core–shell QDs,[1] studies of type-II QDs are relatively rare. Recently, based on a colloidal template, a seminal work on the chemical syntheses of type-II CdTe/CdSe (core–shell) and CdSe/ZnTe (core–shell) QDs using $Cd(CH_3)_2$ as a Cd precursor has been reported.[2] This colloidal template approach is crucial in that it provides both feasibility and versatility toward further chemical modification. In one approach, we have recently reported the synthesis of CdSe/ZnTe (core–shell) type-II QDs via a safer precursor (CdO) and studied their corresponding excited-state relaxation dynamics.[3] In another approach, CdTe/CdSe type-II QDs have been exploited as near-infrared (NIR) dyes for biomedical imaging in living

[*] C.-Y. Chen, C.-T. Cheng, C.-W. Lai, Y.-H. Hu, Prof. Dr. P.-T. Chou
Department of Chemistry, National Taiwan University
Taipei 106 (Taiwan)
Fax: (+886) 2-2369-5208
E-mail: chop@ntu.edu.tw
Y.-H. Chou, Prof. Dr. H.-T. Chiu
Department of Applied Chemistry, National Chiao Tung University
Hsinchu 300 (Taiwan)
Fax: (+886) 35-571-4732
E-mail: htchiu@cc.nctu.edu.tw

tissue, by taking advantage of their great photostability and deeper light penetration.[4] From the chemistry viewpoint, one intriguing approach to the type-II structure is to greatly extend the lifespan of the charge separation, so that either the electron or hole floating on the outermost shell region can be further exploited in a variety of applications, among which the use of type-II QDs as a catalyst in redox reactions is of particular importance. In view of this goal, we have carried out the corresponding design strategy and herein report the synthesis and spectral characterization of a CdSe/CdTe/ZnTe (core–shell–shell) type-II QD. As shown in Figure 1, in this case both the valence and conduction bands in ZnTe are well above those in CdTe and form a type of cascade of band edges in the sequence CdSe < CdTe < ZnTe. Upon excitation, the electron and hole are eventually confined in CdSe and ZnTe, respectively. Thus, the lowest-lying elecron/hole combination, thermodynamically, should originate from CdSe (electron) and ZnTe (hole). The rate of recombination is expected to be rather slow because charge separation is enhanced by an intermediate CdTe layer. Thus, in addition to the synthetic challenge and future chemistry perspectives, the associated photophysical properties of CdSe/CdTe/ZnTe (core–shell–shell) type-II QDs are also of great importance.

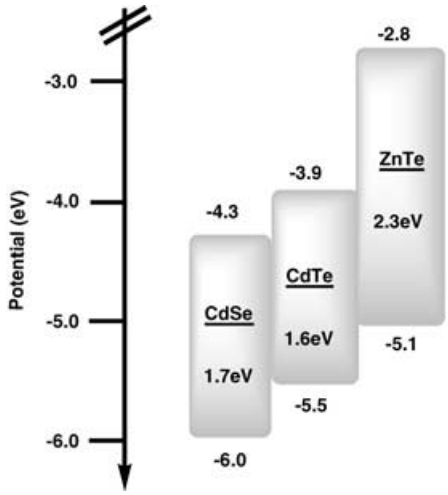

Figure 1. Diagram illustrating the alignment of CdSe, CdTe, and ZnTe band offsets. Note that the energy level of band edges is taken from the bulk properties of the corresponding materials. In addition, subtle changes of the bandgap and, hence, the relative energies in the interfacial regions are neglected in this diagram.

2. Results and Discussion

2.1. Structural Characterization

Figure 2 shows transmission electron microscopy (TEM) images and size histograms of CdSe/CdTe (core–shell) and CdSe/CdTe/ZnTe (core–shell–shell) QDs in which the core–shell QDs are from the same batch. The size histograms of CdSe/CdTe and CdSe/CdTe/ZnTe QDs were established by counting each individual image over 500 particles. Since the CdSe/CdTe/ZnTe QDs were prepared from the same batch of CdSe/CdTe, it is reasonable to assume the same core–shell size. As an indirect approach, the thickness of ZnTe can be estimated by the subtraction of the CdSe/CdTe size from that of the prepared CdSe/CdTe/ZnTe. In Figure 2a, the diameters of the CdSe/CdTe and CdSe/

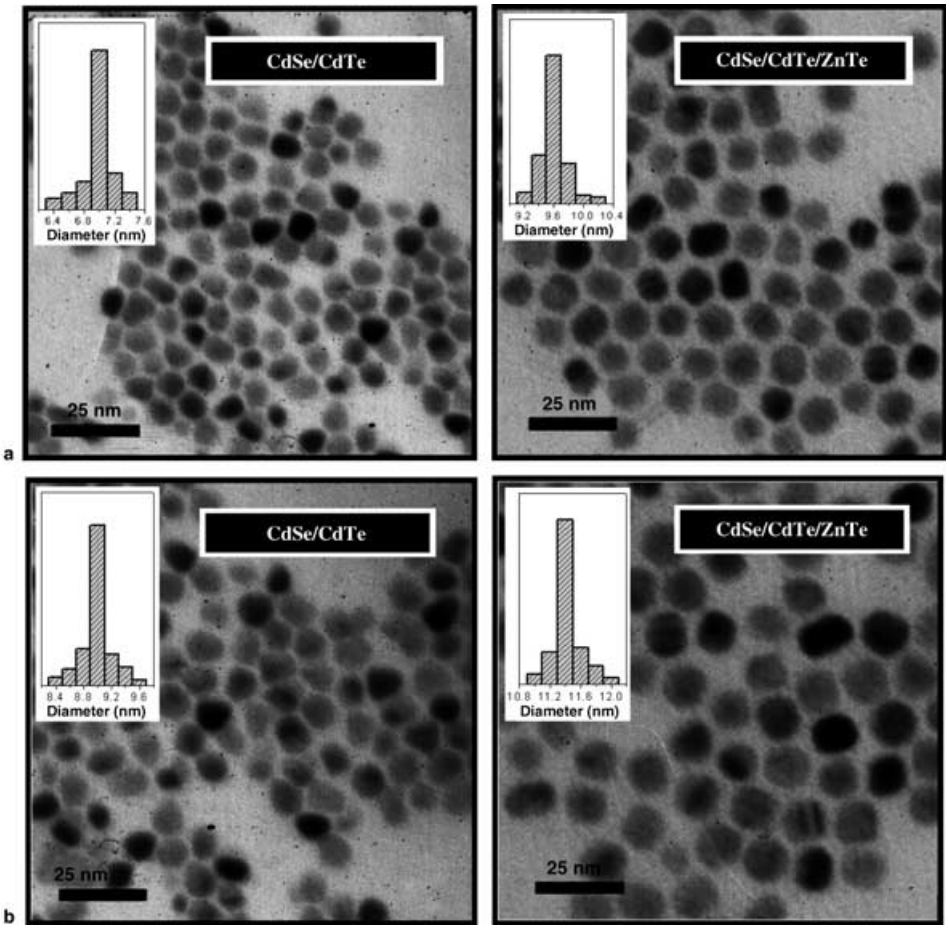

Figure 2. TEM images of the samples with an average of: a) 7.0-nm CdSe/CdTe QDs (left), 9.6-nm CdSe/CdTe/ZnTe QDs (right); b) 9.0-nm CdSe/CdTe QDs (left), 11.4-nm CdSe/CdTe/ZnTe QDs (right). See Table 1 for detailed sizes of core and shell. Insets: Corresponding size histograms made by counting over 500 particles in each sample.

small NANO MICRO

Table 1. Room-temparature photophysical properties of CdSe, CdSe/CdTe, and CdSe/CdTe/ZnTe QDs in toluene.

	Size [nm]	PL, λ_{max} [nm]	Φ_f	τ_f [ns][d]	Radiative lifetime
CdSe	3.4	550	0.28	18 (90)	64 ns
	5.7	648	0.31	22 (85)	71 ns
CdSe/CdTe	7.0[a]	1026	1.2×10^{-3}	29 (82)	24 μs
	9.0[c]	1090	1.0×10^{-3}	31 (80)	31 μs
CdSe/CdTe/ZnTe	9.6[a]	1415	1.5×10^{-5}	150[e]	10 ms
	10.6[b]	1470	1.3×10^{-5}	115	8.8 ms
	11.4[c]	1518	1.1×10^{-5}	120	11 ms

[a] CdSe = 3.4 nm, ZnTe = 1.3 nm (thickness). [b] CdSe = 3.4 nm, ZnTe = 1.8 nm. [c] CdSe = 5.7 nm, ZnTe = 1.2 nm. [d] Percentage of the major photoluminescence (PL) decay component based on two single exponential fits is given in parentheses. [e] A single exponential fit was used due to the small signal-to-noise ratio.

CdTe/ZnTe QDs were an average of 7.0 and 9.6 nm, respectively. Accordingly, the thickness of ZnTe was estimated to be 1.3 nm. Note that the initial CdSe was prepared to be 3.4 nm (see Table 1) in this batch. In another approach, the CdSe core was altered to 5.7 nm. Accordingly, as shown in Figure 2b, the sizes of the CdSe/CdTe and CdSe/CdTe/ZnTe QDs were 9.0 and 11.4 nm, respectively.

The corresponding composition of CdSe/CdTe/ZnTe was characterized by energy dispersive spectroscopy (EDX). As shown in Figure 3a, the appearance of Zn peaks at 1.0 and 8.7 keV, in combination with the decrease in the ratio of Cd to Te in CdSe/CdTe/ZnTe compared to CdSe/CdTe, may indirectly support the formation of a ZnTe shell, although the possibility of alloy formation cannot be ruled out. Furthermore, the X-ray diffraction (XRD) patterns in Figure 3b shows two sets of peaks at faces (100), (002), (101) and (110), (103), (112) for CdSe/CdTe core–shell QDs and reveals the same spectral features for CdSe/CdTe/ZnTe QDs but with slight shifts to a higher scattering angle for the (110), (103), (112) peaks. Interestingly, in contrast to the hexagonal wurtzite structure for CdSe (not shown here),[5] the XRD patterns correspond to the cubic zinc blende rather than the hexagonal wurtzite structure for CdSe/CdTe and CdSe/CdTe/ZnTe nanocrystals. This viewpoint can be supported by the fact that the width of the peaks at around $2\theta = 25^\circ$ is comparable to, or even smaller than, the width of the peaks around 40 and 47°. Moreover, the (103) peaks in the patterns shown in Figure 3b are completely suppressed. The results indicate that the CdSe core transforms into the cubic lattice upon growth of the CdTe shell. We tentatively explain this result as the transformation of CdSe from the hexagonal wurtzite to the cubic lattice structure to fit the growth of the CdTe shell, which results in a more thermodynamically stable structure. Nevertheless, the actual mechanism of structural transformation awaits resolution. Work focused on this issue is currently in progress.

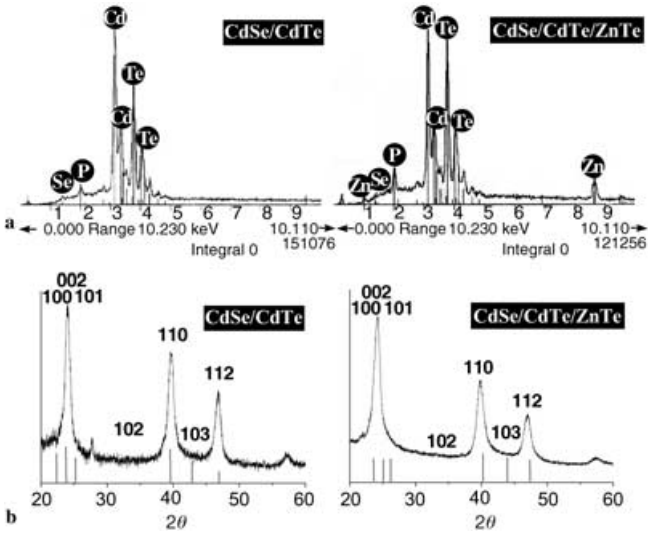

Figure 3. a) EDX characterization of CdSe/CdTe core–shell and CdSe/CdTe/ZnTe core–shell–shell QDs (left and right, respectively). b) XRD data of CdSe/CdTe core–shell and CdSe/CdTe/ZnTe core–shell–shell QDs.

Owing to the similar XRD patterns for these two sets of peaks, the formation of an alloy upon encapsulating ZnTe is not likely. Nevertheless, similar to the results of EDX, the X-ray data could not definitely confirm a core–shell–shell structure. To try and extract more composition information, we performed X-ray photoelectron spectroscopy (XPS) analyses. However, due to the same Te element in both the CdTe and ZnTe shell structures, the characteristic bands associated with either shell–shell or alloy compositions are theoretically the same. This makes XPS analysis impracticable to differentiate core–shell–shell and alloy structures. As an alternative XPS approach, the peak-intensity ratio for elements of the core and shell as a function of the electron takeoff angle may serve as a tool to extract geometrical information about the nanoparticles.[6] Piyakis et al.[7] reported the analysis of spherical Cu nanoclusters by using angle-resolved XPS in combination with Monte Carlo simulation. Accordingly, the XPS method using the peak-intensity ratios may be valid.[8] If the QDs were entirely composed of an alloy, the relative peak intensities for Cd, Se, Zn, and Te would be independent of the electron takeoff angle. Empirically, the ratio of peak intensities at 90 and 54.7° for X-ray sources are estimated to be 0.867, 0.905, 0.900, and 0.863 for Cd($3d_{5/2}$), Se(3d), Zn($2p_{3/2}$), and Te($3d_{5/2}$), respectively.[9] Thus, upon normalizing the Zn peak intensity, the peak intensity ratio for Cd(90°)/Cd(54.7°) is deduced to be 0.96 in the case of an alloy. Deviation from this value is thus expected for a multilayer such as the core–shell–shell structure. On this basis, we have made extensive efforts in angle-tuning studies. Unfortunately, negligible dependence on electron takeoff angle was observed for the ratio of peak intensities. This result may not be surprising for the current CdSe/CdTe/ZnTe structure. On the one hand, the relatively

thin layers of both the CdTe and ZnTe shells, in comparison to the CdSe core, may lead to the peak intensity for Cd mainly being attributed to that of the core, and hence it is not sensitive enough to the angle tuning. On the other hand, as concluded by Piyakis et al.[7] in their study of angle-resolved XPS, if the radius of the particle is larger than the attenuation length of the photoelectron, the intensity may be more or less angle independent. More evidence of the CdSe/CdTe/ZnTe core–shell–shell structure is provided in the following section.

2.2. Photophysical Properties

The absorption and emission spectra of three types of QDs are shown in Figure 4, and the corresponding spectral and dynamic parameters are listed in Table 1. Tuning type-I CdSe (core only) to the type-II CdSe/CdTe QDs significantly alters both the absorption and emission spectra (see Figure 4), in which the transition switches from the core

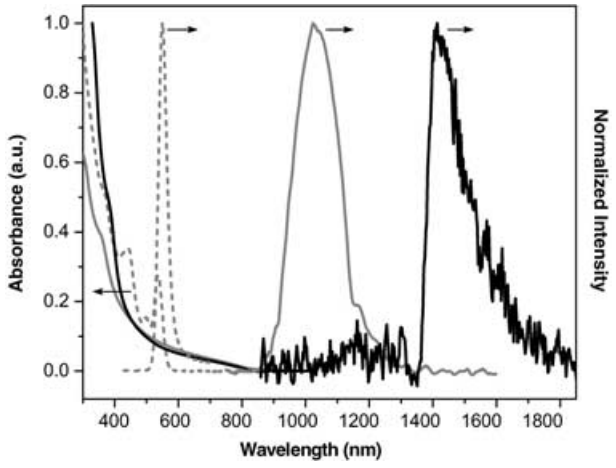

Figure 4. Normalized absorption and emission spectra of CdSe core (3.4 nm, dashed gray line), CdSe/CdTe (3.4/1.8 nm) core–shell (solid gray line), and CdSe/CdTe/ZnTe (3.4/1.8/1.3 nm) core–shell–shell (solid black line) QDs in toluene. See Table 1 for other photophysical parameters.

emission ($\lambda_{em} \approx 550$ nm) in CdSe to the CdSe→CdTe interband emission ($\lambda_{em} \approx 1026$ nm) in the CdSe/CdTe structure. Furthermore, the quantum efficiency ($\Phi_f \approx 1.2 \times 10^{-3}$) of the 1026-nm interband emission is significantly lower than that ($\Phi_f \approx 0.28$) of the corresponding 550-nm core-only emission. The results can be rationalized by the separation of electron and hole into CdSe and CdTe, respectively. Accordingly, a long radiative lifetime, that is, a small radiative rate constant for the electron–hole recombination, is expected. The long-lived hole carrier floating on the surface of CdTe is further subject to either defect trapping or quenching by surrounding stimuli such as colloids, solvent molecules, etc., which results in a significant reduction of the interband emission.

As depicted in Figure 4, the encapsulation of CdSe/CdTe by an additional ZnTe shell, to form a CdSe/CdTe/ZnTe structure, did not cause appreciable changes in the lower-lying absorption spectra. In sharp contrast, however, the characteristic 1026-nm emission in CdSe/CdTe (3.4/1.8 nm) nearly disappeared, accompanied by the appearance of a very weak, long-wavelength emission maximum at 1415 nm. This result may not be surprising, since the introduction of ZnTe to form CdSe/CdTe/ZnTe QDs creates an additional cascade channel for the hole carrier. Upon excitation, if both electron and hole undergo ultrafast transport, the lowest-lying energy gap should be in between the CdSe and ZnTe transition. On this basis, the 1415-nm emission band fits well to the energy gap of 0.8 eV between CdSe and ZnTe predicted from the bulk materials (see Figure 1) and is tentatively assigned to the CdSe→ZnTe transition. However, due to the relatively weak emission intensity, its origin from the deep-trap emission is also possible. We have thus made an attempt to increase the thickness of ZnTe from $\approx$1.3 to $\approx$1.8 nm. As shown in Table 1, the corresponding emission-peak wavelength shifts from 1415 nm (1.3-nm ZnTe) to 1470 nm (1.8-nm ZnTe). In another approach, we altered the CdSe core size from 3.4 to 5.7 nm, while the shell thicknesses for both CdTe and ZnTe, within experimental uncertainty, remained unchanged. As a result, the emission red-shifted from 1415 to 1518 nm. The results correlate well with the increase (decrease) of the ZnTe valence (CdSe conduction) band edge and produce a decrease of the CdSe→ZnTe transition. Due to the systematic variation of the peak wavelength as a function of the ZnTe thickness, the possibility that the 1415-nm band originates from the deep-trap emission can be ruled out. It is also noteworthy that, in general, an alloy composite would give a blue-shift in both emission and absorption edges.[10] Thus, the red-shifts in both the absorption and emission spectra of the CdTe→ZnTe transition, shown in Figure 4 and Table 1, indirectly prove the CdSe/CdTe/ZnTe (core–shell–shell) structure rather than alloy formation.

Table 1 lists the room-temperature emission properties for all three types of QDs with the same core size (and the same shell thickness for CdTe). While CdSe (3.4 nm) gave rise to a tri-*n*-octylphosphine oxide (TOPO) ligand-confined 550-nm emission with quantum efficiency as high as 0.28, the 1026-nm emission in CdSe/CdTe QDs (3.4/1.8 nm) was relatively much weaker with a quantum yield estimated to be 1.2×10^{-3}. Lifetimes (τ_f) for CdSe (3.4 nm) and CdSe/CdTe (3.4/1.8 nm) were further measured to be 18 and 29 ns, respectively. The radiative decay rates, k_r, calculated according to $k_r = \Phi_f/\tau_f$, were then deduced to be 1.6×10^7 s^{-1} (CdSe) and 4.1×10^4 s^{-1} (CdSe/CdTe). Accordingly, the non-radiative decay rates were found to be 4.0×10^7 and 3.4×10^7 s^{-1} for CdSe and CdSe/CdTe, respectively. The >300-fold smaller radiative lifetime for the CdSe→ZnTe emission is attributed to the spatially separated electron–hole recombination (see above). As a result, despite the same magnitude of radiationless decay rates in CdSe/CdTe QDs, their quantum efficiency is much lower than that of CdSe. For the case of CdSe/CdTe/ZnTe QDs, the radiative lifetime of the CdSe→ZnTe transition, which is separated by CdTe, is expected to be enormously long; consequently, the relaxation dynamics may be dominated by the radiationless transition. This viewpoint is supported by the quantum yield of $\approx 1.5 \times 10^{-5}$ for the 1415-nm emission band. As depicted in

NANO MICRO small

Figure 5, the decay trace of the 1415-nm emission band revealed single exponential kinetics, and a lifetime of 150 ns was then extracted. Accordingly, the radiative lifetime of

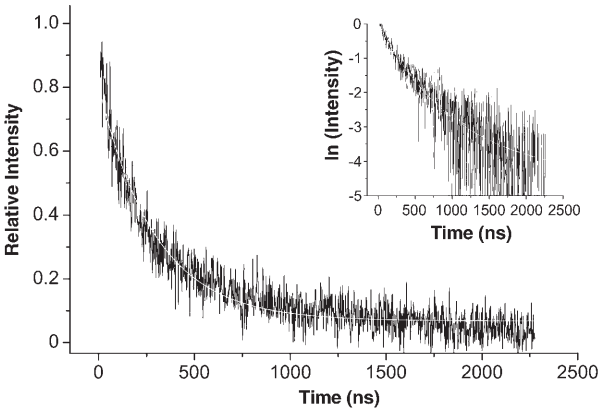

Figure 5. Decay profile of CdSe/CdTe/ZnTe (3.4/1.8/1.3 nm) core–shell–shell QDs in toluene monitored at 1400 ± 20 nm (λ_{ex} = 532 nm). In this decay profile a < 6-ns decay component, resulting from the scattering of fundamental laser light (1064 nm), has been removed. Inset: the logarithm of emission intensity and its first-order linear fit (white line). Note that the decay (k) was fitted by $Ae^{-kt}+B$, where A is the emission intensity at $t=0$ and B is an offset value due to the intrinsic nonzero baseline in the NIR detection system. A similar offset was seen in the blank cuvette filled with solvent only. In this approach, k was fitted as 6.7×10^3 s^{-1} ($\tau_f \approx 150$ ns).

the CdSe→ZnTe emission was deduced to be as long as ≈10 ms. Similar radiative decay times in the range of milliseconds were obtained for CdSe/CdTe/ZnTe QDs upon varying the size of either the CdSe core or the ZnTe shell (see Table 1).

One interesting feature is that the 1026-nm (CdSe→CdTe) emission observed in CdSe/CdTe (3.4/1.8 nm) disappeared in the CdSe/CdTe/ZnTe structure. Upon careful examination of the emission spectra associated with CdSe/CdTe/ZnTe, a trace emission in the region of 1100–1250 nm with $\lambda_{max} \approx 1150$ nm cannot be neglected. By taking account of the subtle interfacial interaction and lattice mismatch, which may cause slight changes of the band edges, it is reasonable to assign this weak band to the CdSe→CdTe interband emission (1026 nm) observed in CdSe/CdTe QDs. However, in view of the bandgaps associated with the CdSe/CdTe/ZnTe structure (Figure 1), one cannot eliminate the possibility that the emission originates from a CdTe→ZnTe transition (1.2 eV in bulk) or from a mixing of CdSe→CdTe and CdTe→ZnTe due to the accidental degeneracy between these two transition gaps (1.2 eV in bulk, see Figure 1). We made efforts to resolve the relaxation dynamics of the extremely weak 1150-nm emission. However, the decay rate was too fast to be resolved by our NIR system, which has a response time of ≈50 ps. It is reasonable to assume a similar radiative lifetime for the CdSe→CdTe emission between CdSe/CdTe and CdSe/CdTe/ZnTe QDs. By taking 24 μs and $<10^{-6}$ for the radiative lifetime and quantum yield, respectively, for the 1150-nm (CdSe→CdTe) emission, an observed lifetime of <25 ps is obtained, which is consistent with the irresolvable experimental relaxation dynamics. If the decay of the CdSe→CdTe emission is dominated by the electron–hole separation, the results support ultrafast electron (or hole) transfer in this CdSe/CdTe/ZnTe structure with cascade band edges. In other words, independent of excitation at the CdSe, CdTe, or ZnTe layers, the rates of electron and hole separation are ultrafast, thus resulting in a unique, lowest-lying CdSe→ZnTe emission.

3. Conclusions

The synthesis and characterization of CdSe/CdTe/ZnTe (core–shell–shell) type-II QDs have been achieved. In comparison to the strong CdSe (core only) emission ($\lambda_{max} \approx 550$ nm, $\Phi_f \approx 0.28$), a moderate CdSe→CdTe emission ($\lambda_{max} \approx 1026$ nm, $\Phi_f \approx 1.2\times10^{-3}$) for CdSe/CdTe (core–shell) and rather weak CdSe→ZnTe interband emission ($\lambda_{max} \approx 1415$ nm, $\Phi_f \approx 1.5\times10^{-5}$) were resolved for the CdSe/CdTe/ZnTe structure (3.4/1.8/1.3 nm). Capping CdSe/CdTe with ZnTe results in a distant electron–hole separation between CdSe and ZnTe via an intermediate CdTe layer. In the case of the CdSe/CdTe/ZnTe structure (3.4/1.8/1.3 nm), a lifetime as long as 150 ns was observed for the CdSe→ZnTe 1415-nm emission. The result further indicates an enormously long radiative lifetime of ≈10 ms due to the spatial separation of electron and hole by the CdTe intermediate layer. In the case of the CdSe/CdTe/ZnTe structure, upon excitation, the float of long-lived charge separation may serve as an excellent hole carrier for catalyzing the oxidation reaction. Attempts have also been made to synthesize the ZnTe/CdTe/CdSe type-II QDs, in which the order of band edges is reversed with respect to the CdSe/CdTe/ZnTe structure, so that the electron can be floated in the CdSe layer to carry out the reduction reaction. However, at this stage this pathway failed due to the difficulty in synthesizing QDs with a ZnTe core. Work focused on circumventing this obstacle is currently in progress.

4. Experimental Section

Chemicals: Tri-*n*-octylphosphine oxide (TOPO, 99%, Aldrich), tri-*n*-butylphosphine (TBP, technical grade 98%, SHOWA), di-*n*-octylamine (DOA, 98%, ACROS), hexadecylamine (HDA, 90%, TCI), CdO (99.99%, Strem), selenium (Se) powder (99.5%, 200 mesh, Aldrich), $CdCl_2$ (99.99%, Aldrich), tellurium (Te) powder (99.8%, 200 mesh, Aldrich), and zinc stearate (Riedel-deHaën) were used as received.

Preparation procedures: Preparation of the CdSe core from CdO was carried out according to a method previously reported by Peng and Peng[11] with a slight modification. Briefly, an injection solution containing Se (0.079 g, 1 mmol) was prepared in a glovebox by dissolving Se powder in TBP (0.3 mL). The Se injection solution was then removed from the glovebox in a vial sealed with a rubber subseal. A mixture of CdO (0.0128 g, 0.10 mmol) and stearic acid (0.114 g, 0.40 mmol) was heated in a three-necked flask to 140 °C under an Ar flow. After the CdO was completely dissolved, the mixture was allowed to cool to

room temperature. TOPO (1.94 g) and HDA (1.90 g) were then added to the flask, and the mixture was heated to 320 °C. The Se solution was quickly injected into the hot solution, and the reaction mixture was cooled to 250–270 °C to allow the growth of the CdSe nanocrystals. Various sizes of CdSe QDs were obtained in the time allowed before termination of the reaction by cooling. CdSe QDs were then precipitated out from the growth solution by the addition of methanol. Further purification was performed by centrifugation and reprecipitation twice from methanol.

To prepare the CdTe shell, $CdCl_2$ and Te powder were used as precursors. In a typical protocol to obtain the CdSe/CdTe core–shell nanoparticles, the precipitated CdSe QDs (0.020 g) were dispersed in TOPO (2.20 g) and HDA (1.26 g) before being heated to 200 °C. In addition, $CdCl_2$ (0.117 g) was dissolved in TBP (3 mL) by gentle heating (ca. 80 °C). After cooling to room temperature, the resulting 0.2 M solution was mixed with Te (3 mL, 0.2 M) in TBP. This mixture was injected with a syringe pump within 1.5 h into the reaction flask containing the core nanocrystals at ≈200 °C. After the addition was completed, the crystals were annealed at 200 °C for an additional 1–1.5 h. Core–shell nanoparticles of various sizes were obtained by adjusting the concentrations of $CdCl_2$ and Te in TBP as well as the corresponding injection periods. The prepared CdSe/CdTe QDs were further purified by centrifugation and reprecipitation twice from methanol.

The CdSe/CdTe/ZnTe (core–shell–shell) QDs were prepared by passivating the CdSe/CdTe with ZnTe. In this approach, Zn stearate and Te powder were used as the precursors. In a typical protocol to obtain the CdSe/CdTe/ZnTe core–shell–shell nanoparticles, the precipitated CdSe/CdTe QDs (0.020 g) were dispersed in TOPO (2.20 g) and HDA (1.26 g) prior to refluxing. In addition, Zn stearate (0.379 g) was dissolved in TBP (3 mL) by gentle heating (ca. 80 °C). After cooling to room temperature, the resulting 0.2 M solution was mixed with Te in TBP (3 mL, 0.2 M). This mixture was injected with a syringe pump within 1.5 h into the reaction flask containing the core nanocrystals at 185–190 °C. After the addition was completed, the crystals were annealed at ≈185 °C for an additional 1–1.5 h. Various ZnTe shell thicknesses could be obtained by adjusting the concentrations of Zn stearate and Te in TBP as well as the corresponding injection periods. The resulting CdSe/CdTe/ZnTe QDs were further purified in the same way as the CdSe/CdTe core–shell QDs.

Measurements: The sizes of the QDs were determined with a Hitachi H-7100 transmission electron microscope. Further characterization was performed by powder X-ray diffraction (XRD, model PANalytical X'Pert PRO) and X-ray photoelectron spectroscopy (XPS, model VG Scientific ESCALAB 250). UV/Vis steady-state absorption and emission spectra were recorded with a Hitachi (U-3310) spectrophotometer and an Edinburgh (FS920) fluorimeter, respectively. The NIR emission spectra were obtained by exciting the sample solution under a rectangular excitation configuration using an Ar-ion laser (488 or 514 nm, Coherent Innova 90); the continuous wave was chopped by a mechanical chopper operated at 200 Hz. To minimize the reabsorption effect, the excitation beam was focused as closely as possible to the front wall of the quartz cell. The near-infrared (NIR) emission was measured by a photomultiplier tube (Hamamatzu R5509-72, operated at −80 °C) coupled with a lock-in amplifier (Stanford Research System SR830) and a monochromator (Acton, SpectraPro-275) with the grating blazed at 1200 nm. IR125 with an emission yield of $\Phi \approx 0.11$ ($\lambda_{max} \approx 925$ nm) in dimethyl sulfoxide (DMSO) served as a standard for calculating the emission quantum yield.[12] For the NIR lifetime measurement, the sample was excited by a 532-nm pulse (second harmonic of Nd:YAG laser, 6 ns). The emission trace was detected by a photomultiplier tube (Hamamatzu R5509-72) operated at −80 °C and recorded by a sampling oscilloscope (Tektronix, TDS 3012). An average of 100 shots were taken in the lifetime measurement, unless otherwise specified.

Acknowledgement

We gratefully acknowledge financial support from NSC and National Taiwan University.

[1] a) A. P. Alivisatos, *Science* **1996**, *271*, 933; b) M. Danek, K. F. Jensen, C. B. Murray, M. G. Bawendi, *Chem. Mater.* **1996**, *8*, 173; c) B. O. Dabbousi, J. Rodriguez-Viejo, F. V. Mikulec, J. R. Heine, H. Mattoussi, R. Ober, K. F. Jensen, M. G. Bawendi, *J. Phys. Chem. B* **1997**, *101*, 9463; d) M. Nirmal, L. Brus, *Acc. Chem. Res.* **1999**, *32*, 407; e) H. Mattoussi, J. M. Mauro, E. R. Goodman, G. P. Anderson, V. C. Sundar, F. V. Mikulec, M. G. Bawendi, *J. Am. Chem. Soc.* **2000**, *122*, 12142; f) D. V. Talapin, A. L. Rogach, A. Kornowski, M. Haase, H. Weller, *Nano Lett.* **2001**, *1*, 207; g) P. Reiss, J. Bleuse, A. Pron, *Nano Lett.* **2002**, *2*, 781.

[2] S. Kim, B. Fisher, H. J. Eisler, M. G. Bawendi, *J. Am. Chem. Soc.* **2003**, *125*, 11466.

[3] C. Y. Chen, C. T. Cheng, J. K. Yu, S. C. Pu, Y. M. Cheng, P. T. Chou, Y. H. Chou, H. T. Chiu, *J. Phys. Chem. B* **2004**, *108*, 10687.

[4] S. Kim, Y. T. Lim, E. G. Soltesz, A. M. De Grand, J. Lee, A. Nakayama, J. A. Parker, T. Mihaljevic, R. G. Laurence, D. M. Dor, L. H. Cohn, M. G. Bawendi, J. V. Frangioni, *Nat. Biotechnol.* **2004**, *22*, 93.

[5] G. W. Huang, C. Y. Chen, K. C. Wu, M. O. Ahmed, P. T. Chou, *J. Cryst. Growth* **2004**, *265*, 250.

[6] I. Tunc, S. Suzer, M. A. Correa-Duarte, L. M. Liz-Marzan, *J. Phys. Chem. B* **2005**, *109*, 7597.

[7] K. N. Piyakis, D. Q. Yang, E. Sacher, *Surf. Sci.* **2003**, *536*, 139.

[8] *Practical Surface Analysis: Auger and X-ray Photoelectron Spectroscopy, Vol. 1*, 2nd ed. (Eds.: D. Briggs, M. P. Seah), Wiley, Chichester, **1993**.

[9] C. D. Wagner, J. F. Moulder, L. E. Davis, W. M. Riggs, *Handbook of X-ray Photoelectron Spectroscopy*, Perkin-Elmer Corporation, Physical Electronics Division, Eden Prairie, MN, **1979**.

[10] M. A. Malik, P. O'Brien, N. Revaprasadu, *Chem. Mater.* **2002**, *14*, 2004.

[11] Z. A. Peng, X. Peng, *J. Am. Chem. Soc.* **2002**, *123*, 183.

[12] R. C. Benson, H. A. Jues, *J. Chem. Eng. Data* **1977**, *22*, 379.

Received: July 7, 2005
Published online on October 11, 2005

